Journal of Nuclear Materials 584 (2023) 154563

Contents lists available at ScienceDirect

Journal of Nuclear Materials

journal homepage: www.elsevier.com/locate/jnucmat

Positron annihilation study of the reactor pressure vessel model steels irradiated in the high flux reactor

Vladimir Krsjak [a,b,*], Stanislav Sojak [a,b], Martin Petriska [a], Branislav Stribrnsky [a], Robert Hinca [a], Matus Huska [a], Vladimir Slugen [a], Murthy Kolluri [c], Oliver Martin [d], Jarmila Degmova [a,b]

[a] Slovak University of Technology in Bratislava, Faculty of Electrical Engineering and Information Technology, Institute of Nuclear and Physical Engineering, Ilkovicova 3, Bratislava 812 19, Slovakia
[b] Slovak University of Technology in Bratislava, Faculty of Materials Science and Technology, Advanced Technologies Research Institute, Jana Bottu 2781/25, Trnava 917 24, Slovakia
[c] Nuclear Research & Consultancy Group (NRG), Petten, the Netherlands
[d] European Commission, Joint Research Centre, Directorate G – Nuclear Safety & Security, Petten, the Netherlands

HIGHLIGHTS

- Extensive positron annihilation experiments were performed on twelve RPV model steels with a parametric variation of Ni and Mn.
- A chemical composition factor was proposed to assess the synergistic effect of the Ni, Mn, Si and Cu.
- Apparent correlation was observed between the positron trapping at radiation-induced vacancy-type defects and the Ni and Mn content.
- The effect of Si and Cu was found to be less pronounced, and the concentration of vacancy-type defects seems to anti-correlate with their content.

ARTICLE INFO

Keywords:
Reactor pressure vessel steels
Neutron irradiation
Displacement damage
Precipitates
Nickel
Manganese
Silicon
Positron annihilation spectroscopy
Late blooming effect

ABSTRACT

Twelve reactor pressure vessel (RPV) model steels with parametric variation of alloying elements Ni and Mn were characterized by means of positron annihilation spectroscopy before and after irradiation at the High Flux Reactor (HFR) to ~0.18 dpa at an average temperature of 286 °C. Two independent positron annihilation lifetime spectrometers (PALS) and one coincidence Doppler broadening spectrometer (CDBS), used in the post-irradiation examination, provided a substantial amount of experimental data used to characterize the vacancy-type defects and their agglomerations in the studied materials. The obtained results show an apparent increase in the positron trapping at vacancy-type defects after irradiation, with the concentration of the radiation-induced vacancy-type defects increasing with the Ni and Mn content. The effect of Si and Cu was found to be less pronounced, and the concentration of vacancy-type defects seems to anti-correlate with their content. In addition to open-volume vacancy-type defects, the PALS technique enabled a quantitative estimation of the dislocation-type defects, where only a modest increase in density was observed after the irradiation at the given temperature.

1. Introduction

Since nuclear power became an integral part of the energy mix and the best low-emission solution to cover the base load power supply, the question of the safe extension of their operating lifetime became current. The post-Fukushima scrutiny of the nuclear industry and the cheap gas prices in the 2010s practically ended the nuclear renaissance that emerged in the early 2000s. Today's energy crisis and the foreseen market prices for electricity in the next decade shed new light on the potential of the operation of the existing nuclear units beyond their original design life [1].

While the development of the next generation of nuclear power reactors aims toward substantially better inherent and passive safety, the current fleet of pressurized water reactors (PWRs) boasts with more than 18 000 reactor years of experience [1]. This experience can undoubtedly provide a guideline for a decision on the extension of the operating

* Corresponding author at: Slovak University of Technology in Bratislava, Faculty of Electrical Engineering and Information Technology, Institute of Nuclear and Physical Engineering, Ilkovicova 3, Bratislava 812 19, Slovakia.
E-mail address: vladimir.krsjak@stuba.sk (V. Krsjak).

https://doi.org/10.1016/j.jnucmat.2023.154563
Received 1 April 2023; Received in revised form 3 June 2023; Accepted 5 June 2023
Available online 12 June 2023

licenses of some of today's reactors in a so-called long-term operation (LTO) regime [2]. In most energy markets, LTO is the cheapest option for generating electricity on a Levelized Cost of Electricity (LCOE) basis and is expected to stay that way for decades to come. Part of the reason that the LTO of existing nuclear power plants (NPPs) is so attractive is that recent experience with a new build in the USA and Europe has seen projects run dramatically over time and budget. However, as existing plants will eventually have to close, LTO cannot be considered as a replacement for the new nuclear build. LTO is fundamentally a stopgap measure and requires less investment.

One of the critical factors in assessing LTO is the embrittlement of the irreplaceable reactor pressure vessel (RPV) due to its exposure to neutron fluences during operation. The fundamental mechanism of embrittlement is the obstruction of dislocation motion caused by various types of nanometric defect structures that develop in the microstructure of the RPV steel exposed to high levels of neutron irradiation. Consequently, the yield stress of the material increases (radiation-induced hardening) along with the reduction of the ductility and the increase of the ductile-to-brittle transition temperature (DBTT) [3]. While the major role in these mechanisms is played by precipitates of solute atoms such as Ni, Mn, and Cu, the radiation-induced point defects and their agglomerations significantly affect the evolution of the microstructure and the formation of the precipitates. In addition to Ni and Mn, studies of RPV steels in surveillance programmes confirmed the presence of clusters rich in Si formed after irradiation [4]. Silicon, used in steels to control the tempering of martensite, is also known to inhibit the precipitation of cementite [5]. In addition to the matrix damage, formation of Cu-rich precipitates (CRP) and Mn-Ni-rich precipitates (MNP), P segregation on grain boundaries was found to be critical mechanism involved in RPV embrittlement. Unlike the other mechanism, P segregation is classified as 'non-hardening' (non-hardening embrittlement), since it is not detectable with conventional hardness tests [6].

To determine the synergistic role of some particular elements in the embrittlement process, compositionally tailored steels were produced and irradiated to high neutron fluences at the High Flux Reactor (HFR) Petten, The Netherlands as part of the LYRA-10 experiment [7]. The post-irradiation examination (PIE) has been conducted by an international consortium within the Horizon 2020 project STRUMAT-LTO [8]. As a part of the microstructural characterization of the irradiated materials, unique experiments by positron annihilation spectroscopy were proposed. This paper reports the first results obtained from positron annihilation lifetime spectroscopy (PALS) and coincidence Doppler broadening spectroscopy (CDBS) experiments performed on 12 RPV model steels in the as-received state and after neutron irradiation. While several comprehensive studies were published on positron annihilation experiments on RPV steels in the past [9–18], the present study reports a unique fission neutron irradiation experiment in terms of the investigated materials as well as in terms of the PIE.

2. Materials and methods

2.1. Materials and sample preparation

Twelve model steels with the parametric variation of alloying elements, were derived from compositions typical for WWER-1000 (MS-A to MS-H) and PWR RPV (MS-K to MS-N) materials (Table 1). The WWER-1000 steels contain a higher amount of some specific elements such as Cr, Mo, Ni and V when compared to typical "western" PWR materials [19].

A pair of identical samples from each material with dimensions of 10×6 × 0.35 mm was irradiated within the LYRA-10 capsule together with other samples prepared for mechanical and microstructural testing and proposed later to be investigated in the frame of the STRUMAT-LTO project. After the irradiation and basic ultrasonic cleaning, the samples were delivered to the Institute of Nuclear and Physical Engineering (INPE), the Slovak University of Technology in Bratislava, for PIE using PAS techniques. The presented experiments were performed after mechanical polishing, followed by ultrasonic cleaning. In addition to the investigated materials, several electropolished calibration samples were used to estimate the source contribution and the apparatus resolution function. During the PAS measurements, the positron source was placed in between the two samples of the same material and the whole

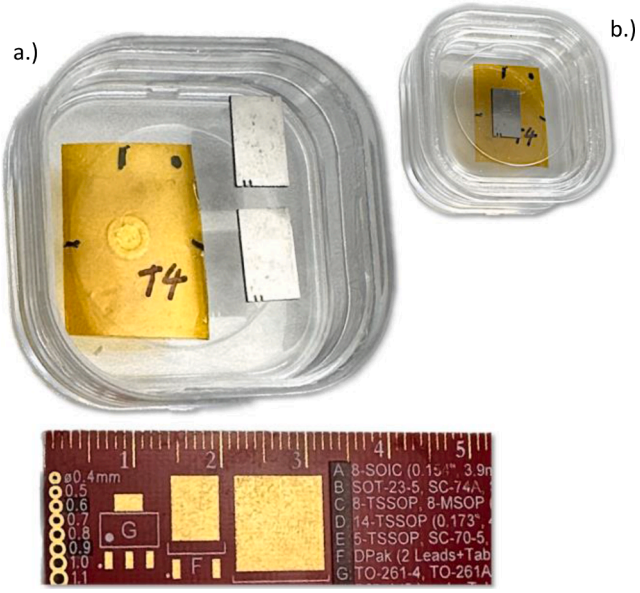

Fig. 1. A typical pair of WWER-1000 model steel samples (MS - H) with a kapton-encapsulated positron source before (a) and after (b) assembling in a sandwich configuration. Note: all samples were identified with characteristic cut marks at the edge of the short side of the rectangle sample.

Table 1
Chemical composition of the studied materials. The level of table cell shading indicates different levels of the concentration of the individual elements.

Model Steel	C	Si	Mn	Cr	Ni	Mo	V	Cu	S	P
MS - A	0.11	0.28	0.43	2.22	0.02	0.71	0.1	0.09	0.008	0.01
MS - B	0.11	0.26	0.38	2.19	0.99	0.7	0.1	0.1	0.008	0.01
MS - C	0.12	0.24	0.38	2.13	2	0.69	0.1	0.1	0.008	0.01
MS - D	0.11	0.23	0.83	2.13	2	0.68	0.1	0.09	0.008	0.009
MS - E	0.12	0.33	0.77	2.16	1.02	0.7	0.1	0.1	0.008	0.009
MS - F	0.12	0.33	1.37	2.15	1.02	0.7	0.1	0.1	0.008	0.01
MS - G	0.11	0.32	1.36	2.06	1.99	0.69	0.1	0.1	0.008	0.009
MS - H	0.12	0.51	1.31	2.07	2	0.69	0.1	0.1	0.008	0.01
MS - K	0.17	0.35	0.78	0.1	0.58	0.64	–	0.07	0.005	0.009
MS - L	0.18	0.35	0.77	0.08	0.96	0.63	–	0.05	0.005	0.01
MS - M	0.16	0.37	0.74	0.09	1.9	0.61	–	0.05	0.005	0.01
MS - N	0.16	0.33	1.27	0.07	1.97	0.63	–	0.06	0.005	0.01

sandwich was contained in a polymer membrane box (Fig. 1).

2.2. Irradiation experiment

The irradiation experiment at the HFR Petten ran for 16 HFR cycles (~467 full power days at a nominal reactor power level of 45 MW) to achieve a nominal fast neutron fluence (E>1 MeV) of 1.11 × 10^{20} n. cm^{-2} at an average temperature of 286 °C. The received fluence corresponds to ~89 effective full power years of a PWR reactor operation and to displacement damage ~0.18 dpa. More details on the irradiation experiment can be found in [8].

2.3. Gamma spectroscopy

A gamma spectroscopy characterization and dosimetry measurements of all irradiated samples was conducted to assess a potential effect of 60-Co on the PALS measurements (Table 2). The post-irradiation cooling at the time of the gamma measurements was about 46 months. While the false start-stop signals are effectively minimized by using of two stop detectors in a coincidence mode, the background noise and the peak-to-background can be still affected by the activity of radioisotopes produced in the steel during the irradiation. As can be seen in Fig. 2, both the activity and the corresponding measured dose rate are roughly proportional to the total concentration of all elements listed in Table 1. Although the 60-Co was expected to be primarily produced from Fe, its activity is not inversely proportional to the total content of non-ferrous alloying elements.

2.4. Positron annihilation spectroscopy

Two different techniques and three independent spectrometers were used to characterise the model steel samples in the as-received (reference) state and after neutron irradiation. Two positron lifetime spectrometers were used with two different positron sources. While both sources are based on a Kapton-encapsulated ^{22}Na radioisotope and have the same design, some small variations of the source activity and the source contribution (fraction of positrons stopped in the encapsulation material) were observed. The actual source contribution, inevitable particularly in the PALS spectra evaluation, was obtained independently as a free parameter (global variable) for the set of 12 reference and 12 irradiated samples, respectively. It was found to be 24.0 ± 0.7% for the source No.1 (marked as T3 and used in PALS 1 spectrometer coupled with CDBS spectrometer) and 26.5 ± 0.4% for the source No.2 (marked as T4 and used in PALS 2 spectrometer). In both sources, ~87% of this contribution was from the annihilation in Kapton foil (382 ps) and the rest from the annihilation in air or polyethene membrane box (τ = 2.5 – 3 ns), used as a sample holder, respectively.

2.4.1. Positron annihilation lifetime spectroscopy (PALS)

Positron lifetime spectra were acquired using two triple coincidence setups based on DRS4 digitizers. Hamamatsu H3378 photomultipliers with BaF_2 scintillators were assembled by Scionix. The resolution in terms of the full width at half of the maximum, obtained from all fittings as a global free parameter was 163 ± 3 ps. Fig. 3 shows a typical positron lifetime spectrum of a model steel before and after neutron irradiation,

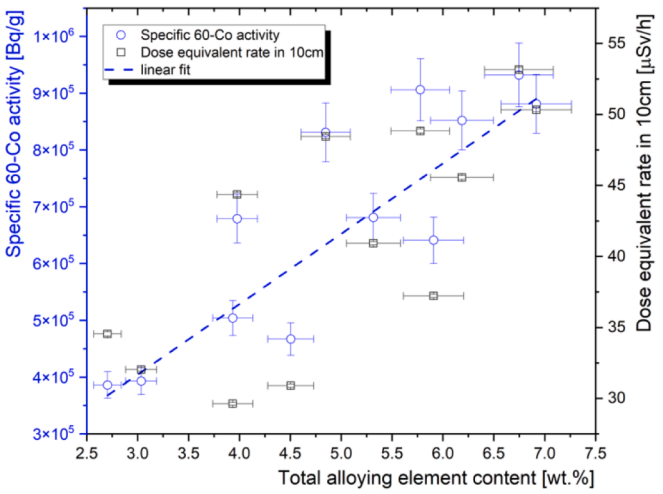

Fig. 2. The total alloying element content in wt.% (left) and the dose equivalent (right) as a function of the 60-Co activity.

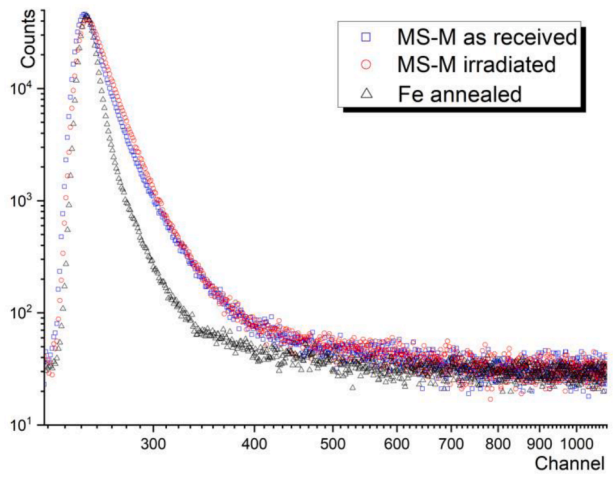

Fig. 3. Typical positron lifetime spectrum of a model steel before and after neutron irradiation.

compared to the defect-free Fe sample. The spectra clearly indicate a more pronounced positron trapping in the irradiated sample, as expected.

The lifetime data were evaluated using the LT10 software [20] as four series of 12 spectra obtained on the reference and irradiated samples respectively, using two independent lifetime spectrometers. The zero channel was found automatically and the region of interest for the fitting was set as - 12 channels and + 1000 channels from the zero channel. The resolution of both spectrometers was 10 ps/channel. A typical spectra decomposition of a reference and irradiated sample can be seen in Fig. 4. Note a significant reduction of the bulk component contribution after the irradiation (describing defect-free matrix annihilation) along with the increase of the 3rd component attributed to

Table 2
Dosimetry data obtained from the PAS samples after neutron irradiation at the time of PAS measurement.

	MS-A	MS-B	MS-C	MS-D	MS-E	MS-F	MS-G	MS-H	MS-K	MS-L	MS-M	MS-N
Dose rate at 10 cm, [uSv/h]	19.3	23.7	23.2	18.9	16.7	15.1	20.6	19.8	12.8	12.8	13.1	12.1
Weight, [g]	0.28	0.29	0.31	0.27	0.26	0.27	0.25	0.27	0.28	0.28	0.26	0.27
Specific activity, Mn-54 [MBq/g]	1.88	1.81	1.64	1.51	1.58	1.39	1.93	1.83	1.84	1.62	1.11	1.33
Uncertainty U_{Mn}, [MBq/g]	0.11	0.11	0.10	0.09	0.10	0.09	0.12	0.11	0.11	0.10	0.07	0.08
Specific activity, Co-60 [MBq/g]	0.679	0.831	0.906	0.852	0.681	0.641	0.932	0.881	0.386	0.393	0.504	0.467
Uncertainty U_{Co}, [MBq/g]	0.043	0.052	0.055	0.052	0.042	0.041	0.056	0.052	0.025	0.025	0.031	0.030

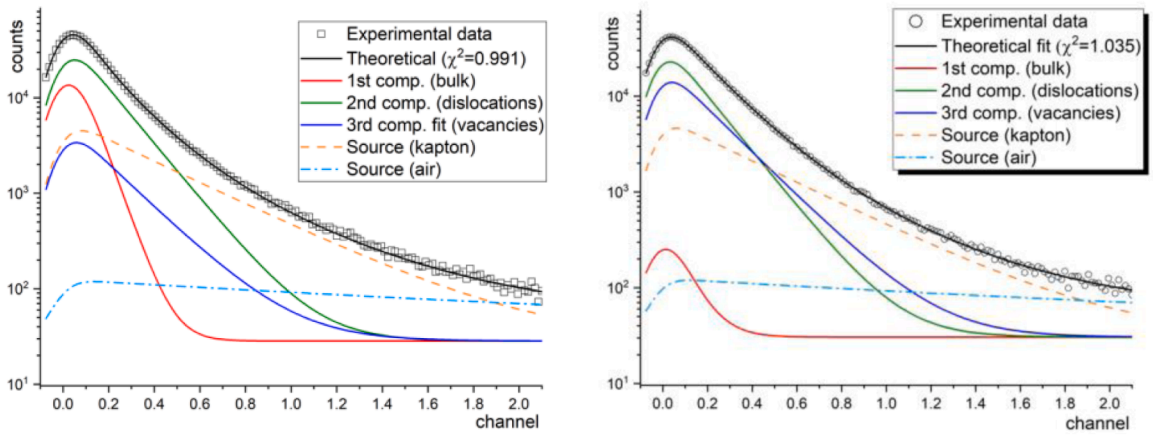

Fig. 4. Positron lifetime spectra of reference (left) and irradiated (right) material (MS-M steel).

vacancy-type defects.

It is important to note, that no significant uncertainty was introduced due to the presence of 60-Co isotope in the irradiated samples. Neither peak-to-background ratio nor the FHWM was found to be notably different in the reference and irradiated samples.

2.4.2. Coincidence Doppler broadening spectroscopy (CDBS)

The coincidence Doppler broadening spectra were acquired using QtCDB2 [21] programme processing the signal from two LN2-cooled HPGe detectors. The analysis of the spectra was performed using CDBTools software [22] developed at the INPE, STUBA. A screenshot from the data treatment of all 24 spectra is shown in Fig. 5. The selection of the range for the S and W parameters, highlighted in red and blue respectively in the figure is discussed in more detail in the next section.

3. Results and discussion

For the evaluation of the positron lifetime spectra, the LT ver.10.0 program [20] was used. In total, four sets of iterations were used independently for the unirradiated samples and irradiated samples measured on the two different lifetime spectrometers. In the first approach, positron mean-lifetime as the statistically most reliable parameter was looked for in the fitting results of two-component spectra decompositions. In this step, the lifetimes of the two components were fixed to 120 ps and 190 ps, attributed to bulk + dislocations and vacancy-type point defects, respectively. This procedure resulted in a fitting variance (global chi-squared reduced) better than 1.05, corresponding to a reasonably good fit. However, obtaining qualitative and quantitative data in terms of dislocation-type defects and vacancy-type defects is problematic in two-component decomposition when more than one type of lattice defect is present. Nevertheless, these results already pointed to a relatively consistent presence of dislocations in both series of samples (reference and irradiated) and the production of small vacancy-type defects in the irradiation experiment. The fact that this model, with two fixed lifetime components, was found suitable for all 24 samples was, to some extent, surprising. It was concluded, moreover, that the size of radiation-induced vacancy clusters does not vary dramatically across the sample set. Despite the feasibility of its application, the two-component model does not enable a quantitative analysis of the radiation-induced vacancy-type defects due to the presence of other intrinsic matrix defects.

In the next step, a three-component fitting model was used for the spectra decomposition. In this model, the first component was attributed to defect-free material bulk (reduced) according to the standard trapping model [23], the second component was attributed to dislocations, and the third component corresponded to radiation-induced

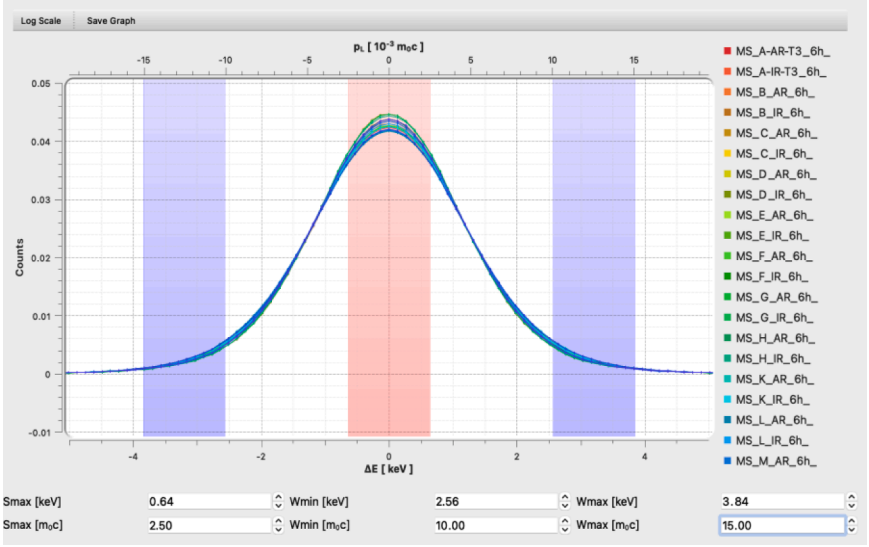

Fig. 5. Screenshot from the CDBTools software used for CDBS data treatment. The selection of the range for the S and W parameters is highlighted in red and blue, respectively. (For interpretation of the references to colour in this figure legend, the reader is referred to the web version of this article.)

vacancy-type defects. The second and third component were fitted as "common free" component, i.e., one value was searched for either of the components in fitting of the whole series of spectra. Unlike the two-component model, this model was used separately for fitting reference and irradiated samples, respectively. This model was found to be slightly worse with reduced chi-squared for some unirradiated samples. For the irradiated samples, the three-component model was generally better or comparable to the two-component model. This can be explained by the low concentration of vacancy-type defects in the unirradiated samples resulting in a low-to-negligible intensity of the third component.

The positron lifetimes and intensities (average or range), obtained from the three-component spectra decomposition are listed in Table 3. The mean positron lifetimes obtained as average values and standard deviations of the two series of fittings corresponding to the two used lifetime spectrometers, are shown in Table 4. It is important to note that after the irradiation, the discrepancy between the 2-component and 3-component model, in terms of positron mean lifetime, decreases from ~16.5 to ~7.5 ps (see Fig. 6). We assume this is due to the more dominant role of the radiation-induced vacancy-type defects in the irradiated samples. These defects were described in both models by a separate lifetime component.

Despite some discrepancy in the results obtained from the two different models, there is a good correlation between the change in the positron mean lifetime after the irradiation in the two decomposition models used.

Considering two major type of positron trapping sites, i.e., lattice defects, the lifetime spectra can be analysed in terms of three exponential components according to Eq. (1).

$$n_d(t) = n_0 \sum_{i=1}^{3} I_i exp\left(-\frac{t}{\tau_i}\right), \quad (1)$$

where n_0 is the number of positrons at time $t = 0$, n_d is the number of positrons at time t, and τ_i and I_i are the lifetimes and intensities of the given components respectively. The lifetimes and intensities corresponding to dislocation-type and vacancy-type defects are functions of the annihilation rates in bulk (λ_B) and defects (λ_{dis}, λ_{vc}) and trapping rates into defects (κ_{dis}, κ_{vc}) according to Eqs. (2) and (3).

$$\tau_2 = \frac{1}{\lambda_2} = \frac{1}{\lambda_{dis}}; I_2 = \frac{\kappa_{dis}}{(\lambda_B - \lambda_{dis} + \kappa_{dis} + \kappa_{vc})} \quad (2)$$

$$\tau_3 = \frac{1}{\lambda_3} = \frac{1}{\lambda_{vc}}; \; I_3 = \frac{\kappa_{vc}}{(\lambda_B - \lambda_{vc} + \kappa_{vc} + \kappa_{dis})} \quad (3)$$

In case the material microstructure contains a relatively high density of small traps such as the presently considered dislocations and vacancies, the trapping rates into these defects are proportional to their concentration (Eq. (4)). In such case it is possible to estimate their number density, which is proportional to the experimentally obtained positron trapping rates κ via a constant called trapping coefficient μ [$m^3\ s^{-1}$].

$$\kappa = \mu N \quad (4)$$

In the case of a dislocation-type defect, attributed to the obtained positron lifetime τ_2 ranging from 136 to 150 ps, a specific positron trapping rate of 6 x 10^{-5} m^2s^{-1} was used. This value was taken from the literature as an average specific trapping rate reported for edge and screw dislocations [10,24]. Since a complementary TEM characterization was not available at the time of publishing this study, the specific type of dislocations was not determined at this point. Based on published literature data, however, we expect edge dislocation or vacancy on edge dislocation to be the prevailing type in the reference samples and small radiation-induced dislocation loops to be the principal dislocation-type defect in the irradiated samples [9,25,26]. As can be seen in Fig. 7, the four PWR model steel K, L, M and N show a slightly lower dislocation density in the unirradiated state. After the irradiation, the dislocation density increases in all studied materials by a factor of 1.3 – 3.1, which can be attributed to the formation of small vacancy-type dislocation loops.

For the quantitative analysis of the radiation-induced vacancy-type defects, the specific trapping rate for monovacancies in iron (1.3 x 10^{-14} m^3s^{-1}) was used. As can be seen in Table 3, the positron lifetime of the third component is somewhat larger for the reference unirradiated samples. The value 199.9 ± 4.0 ps is in fact closer to a positron lifetime in di-vacancy, so the corresponding trapping coefficient (2.6 x 10^{-14} m^3s^{-1}) was used. Here we considered the fact, that the positron trapping coefficient is linearly dependant on the cluster size up to 5–10 vacancies [27,28], so for the same trapping rate the resulting number density is n-times smaller for a cluster of n-vacancies. It is important to note that fittings where the third lifetime component was set as a "local free" were tested, and no material exhibited a lifetime that could be attributed to

Table 3
Positron lifetime and intensities obtained from three-component spectra decompositions using two independent lifetime spectrometers. Note:τ_2 and τ_3 were fitted as common free components while other parameters were set free (local free) in the fittings of the data obtained from each spectrometer.

Samples	τ_1	I_1	τ_2	I_2	τ_3	I_3
Reference	17.0 – 30.7 ps	15.5 - 27.3%	149.5 ± 0.9 ps	69.2 – 84.5%	199.9 ± 4.0 ps	0.0 – 9.9%
Irradiated	2.5 - 13.9 ps	1.5 – 9.3%	135.8 ± 0.9 ps	15.0 – 77.0%	183.1 ± 0.3 ps	14.7 – 83.5%

Table 4
Table 4 Positron mean lifetime (MLT) values obtained from three-component spectra decompositions using two independent lifetime spectrometers.

Sample ID	MLT [ps]	MLT [ps]
A	123.1 ± 1.5	132.1 ± 0.9
B	127.3 ± 2.2	141.7 ± 0.9
C	129.1 ± 0.2	157.4 ± 3.3
D	128.1 ± 2.2	168.3 ± 6.7
E	127.4 ± 1.3	148.7 ± 2.0
F	128.8 ± 1.0	152.3 ± 2.5
G	130.3 ± 1.3	169.5 ± 0.9
H	127.4 ± 1.2	165.1 ± 2.2
K	117.3 ± 1.9	137.8 ± 0.9
L	118.6 ± 1.5	144.9 ± 1.6
M	120.4 ± 1.0	156.4 ± 2.7
N	117.9 ± 2.3	156.9 ± 2.5

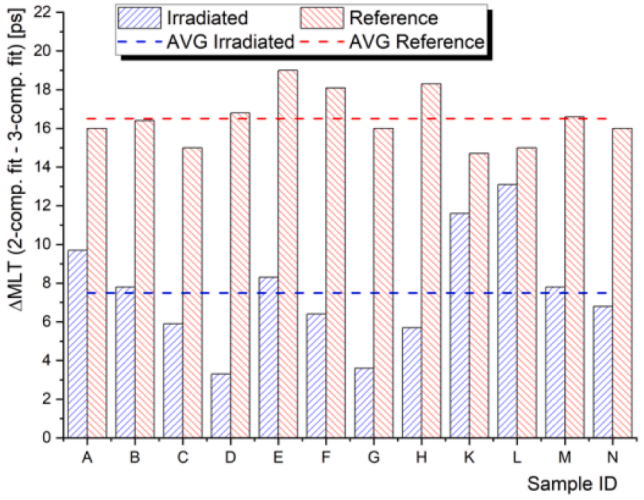

Fig. 6. The increase of positron mean-lifetime obtained from 2-compoenent and 3-compoenent fitting models for irradiated and reference samples.

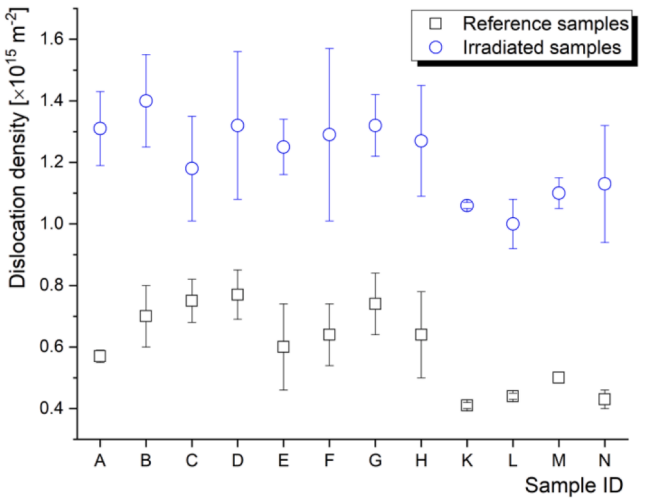

Fig. 7. Dislocation density calculated from positron lifetime spectra of reference and irradiated samples.

larger vacancy clusters. Therefore, the n is not expected to be higher than 2 – 3, and no dependency on the chemical composition of the steel was observed in the fittings of the data. As the overall goodness of fit was not significantly better when using the local free setting, the final data treatment was performed using the "common free" parameter for the two defect components, as discussed above.

As can be seen in Fig. 8, the concentration of vacancy-type defects increases by at least two orders of magnitude in some samples and the resulting number density varies between 1.3 x 10^{24} m^{-3} and 2.6 x 10^{25} m^{-3}. In the unirradiated samples the vacancy component could not be clearly distinguished in the RPV steels (K, L, M, N) and low-alloyed MS-A steel. This suggests the concentration near or below the resolution of the PALS technique in terms of small vacancy-type defects in Fe, which is ~ 8.5 x 10^{21} m^{-3} (0.1 appm) [29]. The effect on chemical composition of the model steel on the concentration of radiation-induced defects is discussed later in the manuscript.

A study similar to the presented one was published by Kocik et al. [10]. Comparable RPV steels irradiated in similar conditions (fluence, flux, temperature) have been characterized by PAS. Unlike in the present study, Kocik et al. observed small clusters of 5 - 6 vacancies in the RPV steel samples after the irradiation. This is a somewhat surprising difference since the two key parameters affecting the growth of vacancy clusters, namely the irradiation temperature and neutron flux, were almost identical to the present experiment. One possible reason for the different results is the relatively large number of interruptions of the present irradiation experiments. These transient regimes could have affected the recombination of the radiation-induced defects by keeping the irradiation target at an elevated temperature for some time without neutron flux being present. Another plausible explanation is that the 260 ps component reported by Kocik et al. was fixed, presuming that the cluster size is relatively constant across the investigated fluency range. This could lead to a possible overestimation of the positron lifetime. Finally, there is a notable difference in the bulk lifetime of the unirradiated materials studied in these two studies. While the positron lifetime of 125 ± 5 ps was obtained in the reference sample in the present study, Kocik et al. reported the positron lifetime in the reference 15Kh2MFA steel 139 ps. This suggests a different microstructure of the materials before irradiation, which could easily lead to the different behaviour of radiation-induced defects in terms of their association with various structures and interfaces of the reference material.

We would like to underline the fact, that the positron lifetime data presented in this work are average values obtained from two independent positron lifetime spectrometers using two different ^{22}Na-based positron sources prepared at INPE laboratories. The error bars presented have been obtained as a standard deviation of two positron lifetime measurement of each of the 24 samples and indicate a very good reproducibility of the PALS data. The obtained results also demonstrate the important role of this technique in the PIE of nuclear structural materials.

The reliability of the so-far presented results can be further supported by the results of the CDBS measurements. Numerous previous published experiments demonstrated an excellent correlation between the positron mean lifetime and Doppler broadening S-parameter, which represents the annihilation with valence/free electrons and increases with positron trapping at defects. Fig. 9 show similar correlation between the PALS and CDBS data.

Similarly, the DBS W-parameter, which represent the annihilation with core electrons, was found to have a reasonably good correlation with the positron lifetime of the first component τ_1. As shown in the Fig. 10, the reduced bulk lifetime component τ_1 describing delocalized positrons reasonably correlates with the W-parameter obtained from the irradiated samples. This correlation justified the used trapping model and validate the values for τ_1, which were obtained independently for each sample.

The choice of momentum ranges of the W parameter was considered

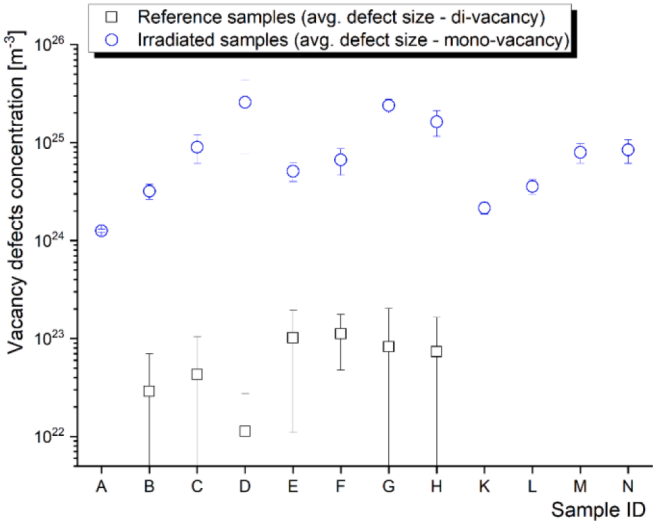

Fig. 8. Vacancy-type defect density calculated from positron lifetime spectra of reference and irradiated samples.

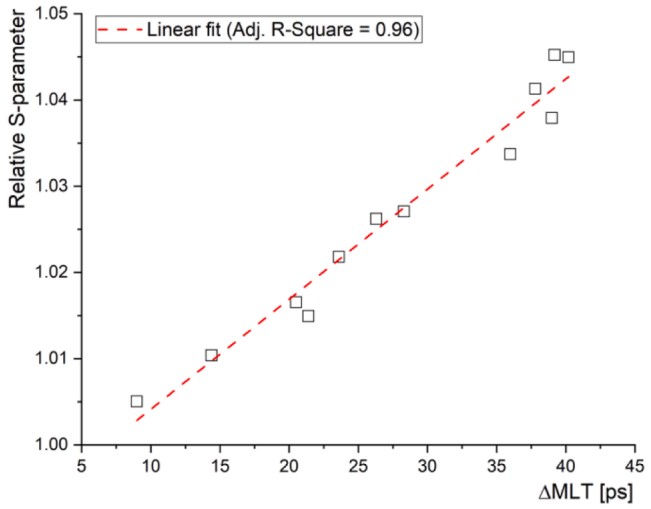

Fig. 9. Relative S parameter vs. positron mean lifetime increase (ΔMLT), obtained from reference and irradiated sample data.

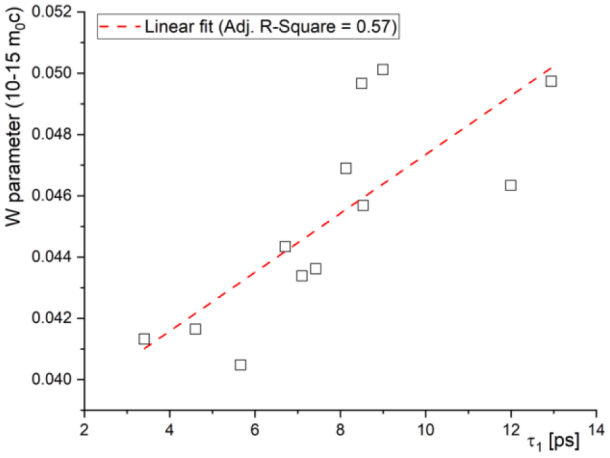

Fig. 10. W parameter vs. reduced bulk-lifetime component obtained for irradiated samples.

in the evaluation of the CDBS data. Fig. 11 compares two different selections of the range, namely the "conventional" range 15–25 m_0c (left) and 10–15 m_0c (right). Since the high-momentum data are rather scattered (exhibiting large error bars) and complicate the interpretation of the CDBS results, we decided to further evaluate the W parameter obtained with the later momentum range. Using a narrower momentum range to characterize the annihilation with core electrons, i.e., the chemical fingerprint of the electron-positron annihilation sites, is a reasonable approach in comparing materials with a parametric variation of several alloying elements. If the chosen range is rather broad, some notable competitive characteristics can diminish each other, resulting in a minor change in the observed W parameter.

The effect of chemical composition on the microstructure of the studied materials was also investigated using the shape of momentum curves. Fig. 12 shows relative momentum curves obtained for all reference samples as a ratio to the MS-A sample with lowest content of alloying elements. Two major bands of the A-H and K-N momentum lines, respectively, can be distinguished in the spectra. From the chemical composition point of view the major difference between the two groups of samples is the chromium content. As discussed above, there is an obvious difference between the positron trapping in these groups in both dislocation density and concentration of point defects. The distinctions between the corresponding CDBS momentum curves are therefore likely a consequence of the lattice defects such as grain boundaries and MC carbides [30]. Due to the low positron affinity (A_+) for Cr comparing to Fe, the preferential trapping of positrons on Cr-associated nano-features is likely negligible.

The potential role of chromium in the behaviour of radiation-induced point defects was further investigated by comparing the S parameter as a function of Cr content for reference and irradiated samples. As shown in Fig. 13, the transition from unirradiated to irradiated condition is neither clear nor robust. It is reasonable to assume that the Cr does not play a distinct role in the radiation stability of the studied model alloys.

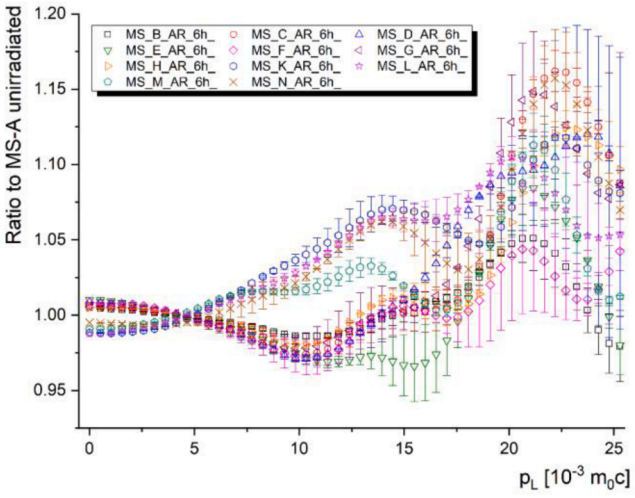

Fig. 12. CDBS momentum curves of the irradiated samples relative to low-alloyed MS-A sample.

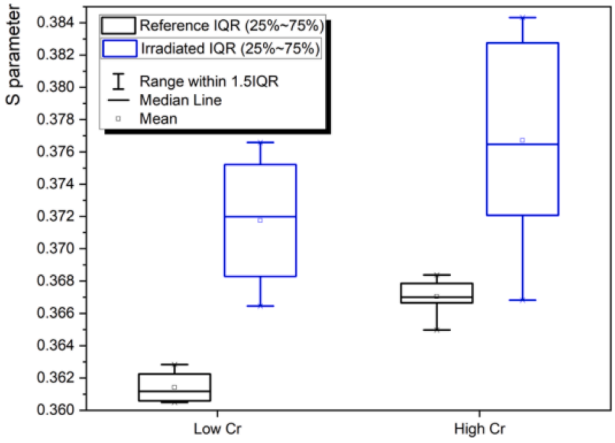

Fig. 13. A comparison of S parameter vs. Cr content in reference and irradiated model steel samples.

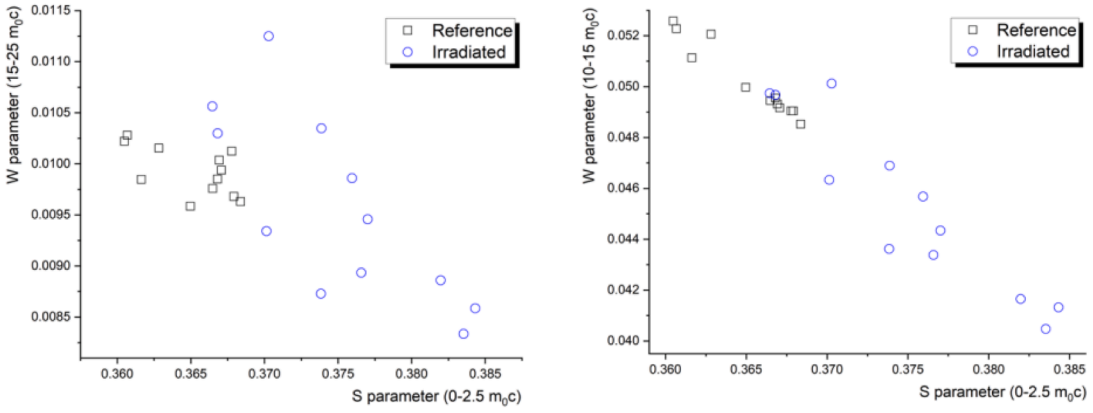

Fig. 11. Comparison of S-W plots for two different momentum ranges of the W parameter.

The chemistry representing the vicinity of the positron annihilation (trapping) sites in the studied materials can be better outlined when the momentum curves of the irradiated samples are plotted against their reference counterparts. Such a plot (Fig. 14) indicates the importance of a suitable selection of the W parameter in the CDBS data evaluation. Unlike the CDBS curves of the unirradiated reference samples (Fig. 12), these data illustrate the change in the chemical environment due to irradiation and possibly distinct types of radiation-induced precipitates. The shape of the ratio curves indicates a certain trend in the mid-momentum region (10–15 m_0c) concerning Ni and Mn. While the low Ni and Mn samples exhibit curves closer to the unity, high Ni and Mn samples show a notable decrease in the ~12 m_0c region. This indicates a possible association of the positron annihilation or trapping sites with Ni and Mn-type precipitates.

Assessing the impact of chemical composition in several model steels and evaluating the role of individual elements is neither easy nor a straightforward task. The effect must reflect not only the typical concentration range of the given element, but also the magnitude of its variation within the sample set. In addition, the experimental approach must consider the sensitivity of the given experimental technique to the individual elements. In the case of positron annihilation spectroscopy, this property is expressed in terms of the affinity of positrons to the corresponding element. If this is higher (more negative) than the affinity of the host lattice (Fe), a cluster or a precipitate rich in this element poses a deeper potential well for the positron.

In the case of the investigated model steels, the average concentration of non-ferrous elements in the material was 4.99 wt.%. As the concentration of the four elements of interest, Ni, Mn, Si and Cu, ranged in different intervals, we introduced a new parameter – range-adjusted concertation $(rac)_i$ to appraise their individual impact on the investigated radiation-induced processes. This parameter was calculated as a ratio of the average concertation of the given element $(avc)_i$ and the product of the average concentration of non-ferrous elements in the material (4.99 wt.%) and the maximal concentration range $(mcr)_i$ of the given element in the studied model steels (Eq. (5)).

$$(rac)_i = \frac{(avc)_i}{4.99 \times (mcr)_i} \tag{5}$$

Hereinafter, i represents Ni, Mn, Si or Cu, respectively. After multiplying the range-adjusted concentration and the positron affinity of the corresponding element, we obtained the composition weighting factor (cwf) according to Eq. (6). As can be seen in Table 5, this can be either positive (Ni and Mn) or negative (Si and Cu), as decided according to the current knowledge of the RPV radiation embrittlement and tested on the fitting of the distribution of the various PAS datapoints (positron mean lifetime, S and W parameter or the obtained concentration of the radiation-induced vacancy-type defects, respectively).

Table 5
Evaluation of the impact of various chemical elements on the formation and clustering of point defects in the studied materials.

Element	Ni	Mn	Si	Cu
Average concentration (avc) [wt.%]	1.37	0.87	0.33	0.08
Maximum concentration range (mcr) [wt.%]	1.98	0.99	0.28	0.05
Range-adjusted concentration (rac)	0.14	0.18	0.23	0.34
Positron affinity rel. to Fe affinity (A_{+rel})	1.16	0.97	1.25	1.81
Assumed sign of the effect: positive (+) negative (-)	+	+	−	−
composition weighting factor (cwf)	1.2	0.8	−0.7	−0.8

$$cwf = \pm\frac{(rac)_{Ni}}{(rac)_i} \times A_{+rel} \tag{6}$$

Finally, we introduced the chemical composition coefficient β to assess the synergistic role of the four elements, according to Eq. (7)

$$\beta\ [wt.\%] = \sum_{1}^{4} (cwf)_i \times c_i \tag{7}$$

where c_i is the concertation of the Ni, Mn, Si or Cu in the given MS sample, respectively. It is important to note that the four elements that impact the radiation damage and are evaluated in detail in this work were not only selected due to their well-known effect on the properties and radiation embrittlement of the RPV steels. In fact, the effect of other elements was also tested in the data interpretation within the present work, but they showed negligible systematic influence on the data distribution.

Based on the current knowledge of the radiation and thermal-induced processes in the RPV steels, we assume that the production, but mainly the survival/recombination rate, of the radiation-induced vacancies are strongly affected by the formation and growth of precipitates. Let us suppose the vacancies are associated with the interfaces of these precipitates. In that case, the trapping (positron lifetime, S parameter) but also the W parameter shall depend on the content of precipitate-forming elements such as Ni, Mn and Cu, as well as on the content of the Si, which is known to be associated with the Ni and Mn precipitates. Fig. 15 shows the dependency of the W parameter on the β coefficient. Since the W parameter is a rather complex function representing the contribution from core electrons, it is reasonable to evaluate it with a minimum number of variable parameters in terms of chemical composition. Let us compare two sets of samples, A-C and K-M, which

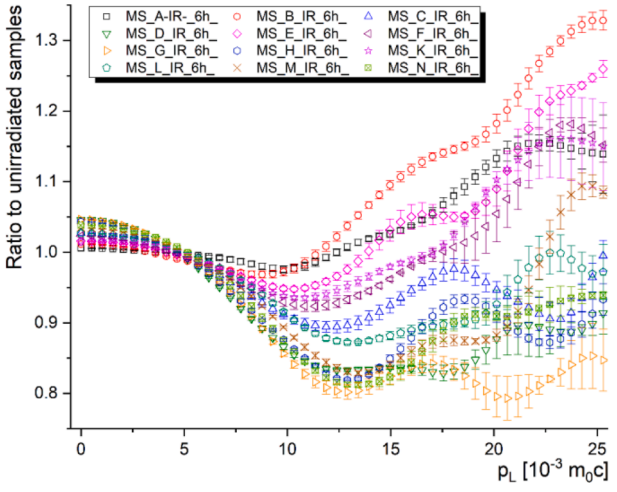

Fig. 14. CDBS momentum curves of the irradiated samples relative to reference samples.

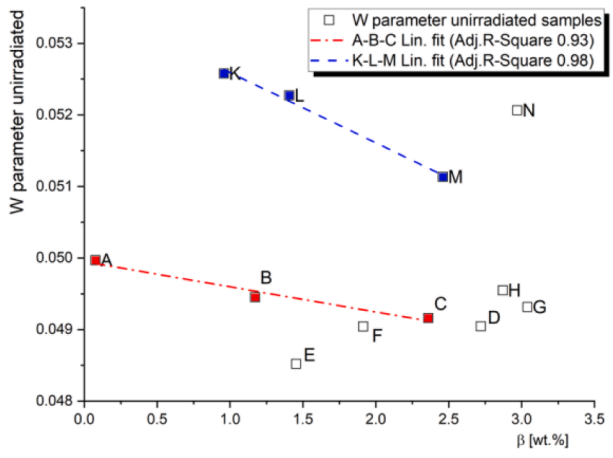

Fig. 15. CDBS W parameter of reference samples plotted as a total content of Ni, Mn, Si and Cu, weighted over their positron affinity.

differ in Ni content while having almost identical concentrations of other alloying elements. One can see a linear dependency on the given chemical factor with a slight difference in the slope between the A-C and K-M lines. We assume this slope is primarily due to Mn and Cr content, whose composition is different in the two sample sets. Similarly, there is one set of three samples, B, E and F, with progressively increasing Mn content and very similar concentrations of other alloying elements. The W parameter, however, does not show any monotonic trend concerning the Mn content in these MS samples. While other lines can be drawn through the data, interpreting such trends would be unclear at best.

After the irradiation we see almost linear dependency of all 12 samples on the chemical composition coefficient β (Fig. 16). This suggests that the formation and growth of precipitates can be a significant factor contributing to the radiation stability of the materials. While the radiation stability is usually addressed separately towards the formation of precipitates and towards the "matrix damage" given by the behaviour of point defects, here we consider these two processes as a single factor which is primarily dependant on the Ni and Mn and secondarily (less contributing factor) on the Si and Cu content.

From the positron lifetime spectra of the irradiated samples, we estimated the concentration of radiation-induced vacancies (considered here as mono-vacancies or di-vacancies). As can be seen in Fig. 17, this concentration increases with the coefficient β and supports the above-discussed interpretation.

As discussed above, the β coefficient was introduced as a sum of the chosen chemical elements with the most pronounced contribution of Ni and Mn. Kolluri et al. [8] reported a synergistic effect between the two elements in the form of a hardening coefficient 1.48*Ni.Mn* [wt.%]. The applicability of this coefficient was tested in the present study, although no meaningful correlation with the production of open-volume defects was found. It is important to note that this outcome neither confirms nor rules out its applicability in the assessment of radiation hardening of RPV steels due to the contribution of various factors, which PAS techniques are not sensitive to (e.g., interstitial-type defects, precipitates of low-A_+ elements etc.).

While the nature of the precipitates cannot be directly obtained from the present data, the matrix damage seems to be associated with the Ni and Mn content. In other words, the obtained data suggest a link between the precipitates of solute atoms such as Ni and Mn and the radiation-induced vacancy-type defects. The increasing content of these alloying elements increases the survival rate of defects produced in displacement damage cascades. Since ultrafine (a few nm in diameter) nickel and manganese enriched precipitates were identified in several experiments on irradiated RPV steels [e.g., [31,32]], their association with point defects is a plausible argument. Moreover, it is generally

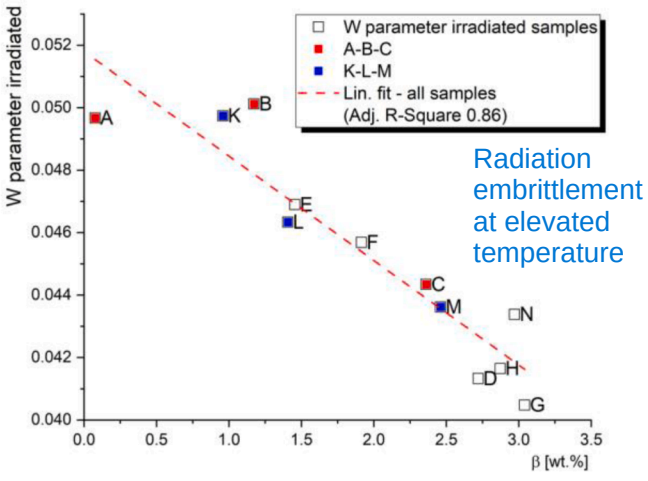

Fig. 16. CDBS W parameter of irradiated samples plotted as a total content of Ni, Mn, Si and Cu, weighted over their positron affinity.

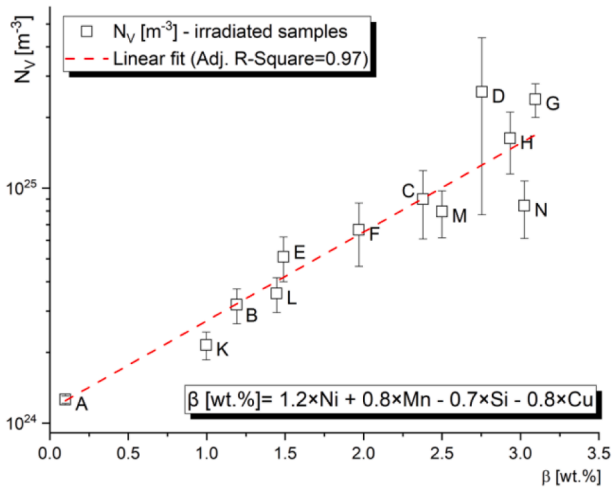

Fig. 17. Concentration of vacancies in the irradiated materials as a function of Ni, Mn, Si and Cu content.

accepted that the presence of Ni in RPV steels increases their sensitivity to neutron-induced embrittlement [33,34]. Although the synergistic effect of Ni and Mn was discovered relatively recently from the APT data [32], it is also fairly accepted in the RPV steels community. Moreover, this study and other APT studies [29] confirm an increased concentration of Si in the Ni and Mn enriched clusters. However, Si can significantly reduce the precipitation kinetics due to its negligible solubility in the cementite phase [5], which can form in thermally aged RPV steels, in particular with high Cu content [35]. This reasonably supports the negative effect of Si in the chemical composition factor proposed in the present study based on the PALS data. Furthermore, Si was reported to suppress void nucleation by extending the transient regime of swelling in steels exposed to harsh radiation environments [36], although this effect is not fully understood yet.

Si supress void formation

Compared to Si, the effect of Cu on the formation of ultrafine precipitates based on Ni and Mn is somewhat unclear. It has been demonstrated that the Cu atoms create small clusters (d 1–2 nm) surrounded by P, Si or Mn atoms under irradiation. The P atoms can even segregate on Cu-clusters. This process poses an embrittlement mechanism in the RPV steel which is accompanied by the increasing yield stress and transition temperature shift after irradiation [14]. While uniformly dispersed Cu-rich precipitates can potentially increase the hardness and strength of the steels [37], the radiation-induced segregation of Cu at the grain boundary is one of the key mechanisms responsible for the embrittlement of RPV steels during reactor operation. Despite the relatively low strength of the CRPs as an obstacle for dislocation glide in neutron-irradiated RPV steels, their contribution is usually highest due to their high number density [38].

Contrary to Ni, Mn and Si, however, the positron affinity is significantly higher for Cu, and Cu-rich precipitates in the Fe matrix could pose a specific type of positron trap. In the case of a high density of such small Cu clusters, these could effectively reduce the positron trapping at vacancy-type defects without changing either the production or the recombination rate of the radiation-induced point defects. In other words, the Cu-rich clusters and/or precipitates can pose a competitive trap to the vacancies associated with Ni and Mn precipitates. Similarly, to Si, this suggests a negative effect of Cu in the chemical composition factor proposed in the present study based on the PALS data. Nevertheless, Cu-rich precipitates are known to mainly contribute to the radiation hardening only in high-Cu RPV steels and relatively low irradiation fluencies [39]. The deleterious effect of Cu on the irradiation-induced embrittlement of RPV steels appears from a Cu content of about 0.04% and becomes very strong above 0.1% [40]. Therefore, the overall effect of Cu in the present study is neither

significant nor straightforward.

Considering the neutron fluence used in the present study, the experimental data could potentially cover the so-called late blooming phase range [41]. This feature of the RPV steels, reported by some authors, refers to a Ni-Mn phase that occurs suddenly after a long "incubation period" in high Ni, low Cu alloys. This supports the model of anticorrelation between the Cu content and matrix damage, discussed above. The present results, however, neither confirm nor exclude the effect of late blooming phases. While the three most-alloyed steels MS-D, MS-G, and MS-H indicate certain level of more rapid formation of radiation damage, the behaviour does not point to any distinct behaviour such as late blooming phase. It is rather reasonable to not make a strong distinction between the matrix damage and the precipitates [39,42].

4. Conclusions

This work presents an extensive positron annihilation experiment on twelve RPV model steels with a parametric variation of alloying elements. The reproducibility of the experimental data was ensured by two independent positron lifetime spectrometers combined with a coincidence Doppler broadening spectroscopy. Based on this unique, extensive data, the following conclusions can be drawn.

- The microstructure of the studied materials can be effectively characterized in terms of two groups of defects – dislocation type and vacancy type defects.
- The obtained dislocation density varies with the alloying element content between 4.0×10^{14} - 7.7×10^{14} cm^{-2} in the unirradiated materials and 1.0×10^{15} – 1.4×10^{15} cm^{-2}. The dislocation density was found to be slightly lower in the PWR steels compared to the VVER model alloys.
- The concentration of vacancy-type defects was found to be significantly lower in the unirradiated PWR steels ($<<1 \times 10^{22}$ m^{-3}) compared to the VVER model alloys (1.1×10^{22} – 1.1×10^{23} m^{-3}). After the irradiation, the vacancies become dominant trapping centers and their concentration increases by almost two orders of magnitude depending on the alloying content.
- A correlation between the matrix damage (radiation-induced vacancy-type defects) and the Ni+Mn+Si+Cu content was found and confirmed by both PALS and CDBS techniques. This suggests an association between the typical precipitates and the behaviour of point defects during irradiation.
- While the increased content of Ni and Mn in the model steels results in higher production/survival rate of radiation-induced defects during irradiation, the Si and Cu contribution seems to have an opposite effect. This can be partially explained by the Si-assisted reduction of the precipitation kinetics in the system and formation of "independent" Cu enriched precipitates which compete the formation of Cu (Ni, Mn, Si) enriched clusters.

This work demonstrates the excellent potential of PAS techniques in terms of qualitative and quantitative characterization of radiation damage in RPV steels. It provides a unique insight into the connection between the matrix damage and the clustering of solute atoms of Ni, Mn, Si and Cu.

CRediT authorship contribution statement

Vladimir Krsjak: Conceptualization, Formal analysis, Writing – original draft, Writing – review & editing. **Stanislav Sojak:** Investigation, Writing – review & editing. **Martin Petriska:** Investigation, Software. **Branislav Stribrnsky:** Investigation, Data curation. **Robert Hinca:** Investigation, Data curation. **Matus Huska:** Resources, Data curation. **Vladimir Slugen:** Writing – review & editing. **Murthy Kolluri:** Writing – review & editing. **Oliver Martin:** Writing – review & editing. **Jarmila Degmova:** Project administration, Funding acquisition, Investigation, Writing – review & editing.

Declaration of Competing Interest

We wish to confirm that there are no known conflicts of interest associated with this publication and there has been no significant financial support for this work that could have influenced its outcome.

Data availability

Data will be made available on request.

Acknowledgement

The authors would like to acknowledge partial support from the Slovak Research and Development Agency grants No. APVV-20-0010, as well as from the European Regional Development Fund, projects No. ITMS2014+: 313011BUH7 and ITMS2014+: 313011W085. The authors further acknowledge financial contributions from the Scientific Grant Agency of the Ministry of Education, Science, Research and Sport of the Slovak Republic and the Slovak Academy of Sciences, grant number VEGA 1/0395/20. This work is part of a project that has received funding from the Euratom research and training programme 2019-2020 under grant agreement No. 945272 (STRUMAT-LTO).

References

[1] M.M. Gospodarczyk, M.N. Fisher, IAEA releases 2019 data on nuclear power plants operating experience. https://www.iaea.org/newscenter/news/iaea-releases-2019-data-on-nuclear-power-plants-operating-experience.
[2] A. Vaya Soler, R. Sainz, A. Meert, J. Lehman, P. Smeekes, M. Colacicco, N. Ueda, M. Chaki, A.G. Dumitriu, E. Serra Sintes, J.E. Lindback, S. Asser, B. Hallbert, S. Bernhoft, A.I. Van Heek, P.E. Pini, K. Nagano, O. Martin, P. Luna, G. Diaz, M. Crozat, A. Lohkov, T. Freeman, J.P. Mathieu, Long-term operation of nuclear power plants and decarbonisation strategies, (2021). https://inis.iaea.org/search/search.aspx?orig_q=RN:52083616 (accessed March 9, 2023).
[3] A.D. Amayev, A.M. Kryukov, M.A. Sokolov, Recovery of the Transition Temperature of Irradiated WWER-440 Vessel Metal by Annealing, ASTM Special Technical Publication, 1993, https://doi.org/10.1520/stp24787s.
[4] G.R. Odette, On the dominant mechanism of irradiation embrittlement of reactor pressure vessel steels, Scr. Metall. 17 (1983), https://doi.org/10.1016/0036-9748(83)90280-6.
[5] E. Kozeschnik, H.K.D.H. Bhadeshia, Influence of silicon on cementite precipitation in steels, Mater. Sci. Technol. 24 (2008), https://doi.org/10.1179/174328408X275973.
[6] M. Brumovsky, 11 - Irradiation hardening and materials embrittlement in light water reactor (LWR) environments, in: P.G. Tipping (Ed.), Understanding and Mitigating Ageing in Nuclear Power Plants, Woodhead Publishing, 2010, pp. 357–373, https://doi.org/10.1533/9781845699956.2.357.
[7] L. Debarberis, B. Acosta Iborra, J. Degmová, A. Zeman, M.A. Fütterer, E. D'Agata, P. Hähner, Unique Irradiation Rigs Developed For the HFR Petten at the JRC-IE: LYRA, Quattro and Fuel Irradiation Facilities, International Atomic Energy Agency (IAEA), Vienna (Austria), 2011.
[8] M. Kolluri, P. ten Pierick, T. Bakker, B.T. Straathof, A.J. Magielsen, Z. Szaraz, E. D'Agata, C. Ohms, O. Martin, Influence of Ni-Mn contents on the embrittlement of PWR RPV model steels irradiated to high fluences relevant for LTO beyond 60 years, J. Nucl. Mater. 553 (2021), https://doi.org/10.1016/j.jnucmat.2021.153036.
[9] J. Čížek, I. Procházka, J. Kočík, E. Keilová, Positron lifetime study of reactor pressure vessel steels, Phys. Status Solidi A Appl. Res. 178 (2000) 651–662, https://doi.org/10.1002/1521-396X(200004)178:2<651::AID-PSSA651>3.0.CO;2-O.
[10] J. Kočík, E. Keilová, J. Čížek, I. Procházka, TEM and PAS study of neutron irradiated VVER-type RPV steels, J. Nucl. Mater. 303 (2002) 52–64, https://doi.org/10.1016/S0022-3115(02)00800-0.
[11] V.I. Grafutin, O. Ilyukhina, V. Krsjak, R. Burcl, P. Hähner, D. Erak, A. Zeman, Study of PRIMAVERA steel samples by a positron annihilation spectroscopy technique, J. Nucl. Mater. 406 (2010) 257–262.
[12] J. Jiang, Y.C. Wu, X.B. Liu, R.S. Wang, Y. Nagai, K. Inoue, Y. Shimizu, T. Toyama, Microstructural evolution of RPV steels under proton and ion irradiation studied by positron annihilation spectroscopy, J. Nucl. Mater. 458 (2015) 326–334, https://doi.org/10.1016/j.jnucmat.2014.12.113.
[13] T. Toyama, T. Yamamoto, N. Ebisawa, K. Inoue, Y. Nagai, G.R. Odette, Effects of neutron flux on irradiation-induced hardening and defects in RPV steels studied by positron annihilation spectroscopy, J. Nucl. Mater. 532 (2020), https://doi.org/10.1016/j.jnucmat.2020.152041.

[14] A. Kryukov, L. Debarberis, A. Ballesteros, V. Krsjak, R. Burcl, S.V. Rogozhkin, A. A. Nikitin, A.A. Aleev, A.G. Zaluzhnyi, V.I. Grafutin, O. Ilyukhina, Y.V. Funtikov, A. Zeman, Integrated analysis of WWER-440 RPV weld re-embrittlement after annealing, J. Nucl. Mater. 429 (2012) 190–200.
[15] J.J. Shi, W. Yang, Z.J. Zhu, X.B. Liu, J. Jiang, R.S. Wang, Y.C. Wu, Slow positron beam study of highly irradiated RPV steel under proton and ion impact, Radiat. Phys. Chem. 156 (2019) 199–204, https://doi.org/10.1016/j.radphyschem.2018.11.011.
[16] X. Liu, R. Wang, A. Ren, X. Wang, Y. Wu, C. Zhang, P. Huang, J. Jiang, S. Li, Positron annihilation study of irradiated China domestic A508-3 steels, Procedia Eng. (2012), https://doi.org/10.1016/j.proeng.2011.12.629.
[17] V. Slugeň, H. Hein, S. Sojak, J. Simeg Veterníková, M. Petriska, V. Sabelová, M. Pavúk, R. Hinca, M. Stacho, Evaluation of the reactor pressure vessel steels by positron annihilation, J. Nucl. Mater. 442 (2013), https://doi.org/10.1016/j.jnucmat.2013.08.028.
[18] S.C. Glade, B.D. Wirth, G.R. Odette, P. Asoka-Kumar, Positron annihilation spectroscopy and small angle neutron scattering characterization of nanostructural features in high-nickel model reactor pressure vessel steels, J. Nucl. Mater. 351 (2006) 197–208, https://doi.org/10.1016/j.jnucmat.2006.02.012.
[19] M. Brumovsky, 5 - Embrittlement of reactor pressure vessels (RPVs) in WWER-type reactors, in: N. Soneda (Ed.), Irradiation Embrittlement of Reactor Pressure Vessels (RPVs) in Nuclear Power Plants, Woodhead Publishing, 2015, pp. 107–131, https://doi.org/10.1533/9780857096470.2.107.
[20] D. Giebel, J. Kansy, LT10 program for solving basic problems connected with defect detection, Phys. Procedia 35 (2012) 122–127, https://doi.org/10.1016/j.phpro.2012.06.022.
[21] M. Petriska, V. Slugen, V. Sabelova, S. Sojak, J. Veternikova, QtCDB2 software for coincidence Doppler broadening measurement system, J. Phys. Conf. Ser. 443 (2013), 012086, https://doi.org/10.1088/1742-6596/443/1/012086.
[22] M. Petriska, V. Sabelová, V. Slugen, CDBTools - evaluate positron annihilation coincidence doppler broadening spectrum, in: Positron Annihilation - ICPA-17, Trans Tech Publications, 2017: pp. 71–74. 10.4028/www.scientific.net/DDF.373.71.
[23] A. Seeger, The study of defects in crystals by positron annihilation, Appl. Phys. 4 (1974), https://doi.org/10.1007/BF00884229.
[24] Y. Park, J.T. Waber, M. Meshii, C.L. Snead, C.G. Park, Dislocation studies on deformed single crystals of high-purity iron using positron annihilation: determination of dislocation densities, Phys. Rev. B 34 (1986) 823–836.
[25] E. Kuramoto, T. Tsutsumi, K. Ueno, M. Ohmura, Y. Kamimura, Positron lifetime calculations on vacancy clusters and dislocations in Ni and Fe, Comput. Mater. Sci. 14 (1999), https://doi.org/10.1016/s0927-0256(98)00068-8.
[26] A. Van Veen, H.A. Filius, J. De Vries, K.R. Bijkerk, G.J. Rozing, D. Segers, Hydrogen exchange with voids in tungsten observed with TDS and PA, J. Nucl. Mater. (1988) 155–157, https://doi.org/10.1016/0022-3115(88)90478-3.
[27] R. Krause-Rehberg, H.S. Leipner, T. Abgarjan, A. Polity, Review of defect investigations by means of positron annihilation in II-VI compound semiconductors, Appl. Phys. A Mater. Sci. Process. 66 (1998), https://doi.org/10.1007/s003390050721.
[28] T. Troev, E. Popov, P. Staikov, N. Nankov, Positron lifetime studies of defects in alpha-Fe containing helium, Phys. Status Solidi (C) 6 (2009) 2373–2375, https://doi.org/10.1002/pssc.200982129.
[29] F.A. Selim, Positron annihilation spectroscopy of defects in nuclear and irradiated materials- a review, Mater. Charact. 174 (2021), https://doi.org/10.1016/j.matchar.2021.110952.
[30] G. Brauer, M.J. Puska, M. Sob, T. Korhonen, Positron affinity for precipitates in reactor pressure vessel steels, Nucl. Eng. Des. 158 (1995) 149–156, https://doi.org/10.1016/0029-5493(95)01022-A.
[31] V. Slugeň, A. Zeman, J. Lipka, L. Debarberis, Positron annihilation and Mössbauer spectroscopy applied to WWER-1000 RPV steels in the frame of IAEA High Ni Co-ordinated Research Programme, NDT E Int. 37 (2004) 651–661, https://doi.org/10.1016/j.ndteint.2004.05.001.
[32] M.K. Miller, M.A. Sokolov, R.K. Nanstad, K.F. Russell, APT characterization of high nickel RPV steels, J. Nucl. Mater. 351 (2006), https://doi.org/10.1016/j.jnucmat.2006.02.013.
[33] A.M. Kryukov, Y.A. Nikolaev, A.V. Nikolaeva, Behavior of mechanical properties of nickel-alloyed reactor pressure vessel steel under neutron irradiation and post-irradiation annealing, Nucl. Eng. Des. 186 (1998), https://doi.org/10.1016/S0029-5493(98)00247-7.
[34] G.R. Odette, G.E. Lucas, Embrittlement of nuclear reactor pressure vessels, JOM 53 (2001), https://doi.org/10.1007/s11837-001-0081-0.
[35] J. Zelenty, G.D.W. Smith, K. Wilford, J.M. Hyde, M.P. Moody, Secondary precipitation within the cementite phase of reactor pressure vessel steels, Scr. Mater. 115 (2016), https://doi.org/10.1016/j.scriptamat.2015.12.039.
[36] B. Esmailzadeh, A. Kumar, F.A. Garner, The influence of silicon on void nucleation in irradiated alloys, J. Nucl. Mater. (1985) 133–134, https://doi.org/10.1016/0022-3115(85)90216-8.
[37] W. Lv, W. Jin, L. Yan, X. Pang, H. Yang, K. Gao, Interaction between Cu and Cr coadsorption on MnS inclusions in low alloy steels, Appl. Surf. Sci. 471 (2019), https://doi.org/10.1016/j.apsusc.2018.11.228.
[38] F. Bergner, F. Gillemot, M. Hernández-Mayoral, M. Serrano, G. Török, A. Ulbricht, E. Altstadt, Contributions of Cu-rich clusters, dislocation loops and nanovoids to the irradiation-induced hardening of Cu-bearing low-Ni reactor pressure vessel steels, J. Nucl. Mater. 461 (2015), https://doi.org/10.1016/j.jnucmat.2015.02.031.
[39] S. Kotrechko, Embrittlement of RPV metal under long-term irradiation: state-of-the-art and challenges, Procedia Structural. Integr. (2018), https://doi.org/10.1016/j.prostr.2018.12.003.
[40] International Atomic Energy Agency, Integrity of Reactor Pressure Vessels in Nuclear Power Plants: Assessment of Irradiation Embrittlement Effects in Reactor Pressure Vessel Steels, International Atomic Energy Agency 2009.
[41] F. Bergner, A. Ulbricht, H.W. Viehrig, Acceleration of irradiation hardening of low-copper reactor pressure vessel steel observed by means of SANS and tensile testing, Philos. Mag. Lett. 89 (2009), https://doi.org/10.1080/09500830903304117.
[42] D. Terentyev, L. Malerba, Interaction of a screw dislocation with Cu-precipitates, nanovoids and Cu-vacancy clusters in BCC iron, J. Nucl. Mater. 421 (2012), https://doi.org/10.1016/j.jnucmat.2011.11.037.